Hybrid PWM Scheme for Pole-Phase Modulation Induction Motor Drive Using Carrier-Based Hexagonal and Octadecagonal SVPWM

V. Janaki Ramaiah, *Student Member, IEEE*, and Sivakumar Keerthipati, *Senior Member, IEEE*

***Abstract*—In this article, the advantages of both octadecagonal space vector pulsewidth modulation (SVPWM) and hexagonal SVPWM are explored for a pole-phase modulation (PPM) induction machine (IM) drive applications. In the proposed scheme, a hexagonal SVPWM is used in the low-speed region and octadecagonal SVPWM is used during the high-speed region to achieve better performance over the entire speed range. With this proposed operation, the linear modulation region is enhanced by 9.15% as compared to conventional three-phase SVPWM in the high-speed region. The basic two-level nine-leg inverter is used to excite the nine-phase PPM IM. The finite-element model (FEM) of the PPM IM and inverter structure is simulated using ANSYS Maxwell-2D and Simplorer environment, respectively. The proposed method is verified experimentally on the prototype model of 5-hp nine-phase IM.**

***Index Terms*—Hexagonal space vector pulsewidth modulation (SVPWM), multiphase induction machine (IM), octadecagonal SVPWM, pole-phase modulation (PPM).**

I. Introduction

MULTIPHASE induction machine (IM) has inherent advantages in terms of fault-tolerance, high efficiency, and reduced torque ripple, and also it allows to handle high power with reduced switch ratings [1]–[4]. Pole-phase modulation (PPM) technique helps the multiphase IM to achieve speed-torque characteristics suitable for electric vehicle applications [5], [6]. In general, to achieve high starting torque, the PPM IM is operated in high-pole mode [5]. However, in this mode, the less number of phases leads to more space harmonics and thus results in increased torque ripple [7]–[9]. On the other hand, to achieve high running speed, the PPM IM is operated in low-pole mode. In this mode, the higher number of phases leads to less space harmonics and thus results in reduced torque ripple [4], [10]. There is a requirement for the reduction of torque ripple during high-pole mode and to improve the linear modulation region during low-pole mode.

The space harmonics are more due to the less number of phases during the high-pole mode of operation of PPM IM, which results in increased torque ripple [7]–[9]. To minimize the torque ripple, a carrier phase-shift-based SVPWM control technique is presented in the literature [11], [12] and the same is incorporated in this article during the application of high-pole mode of operation. On the other hand, as the number of phases is more in the low-pole mode of operation, the improvement in the linear modulation region achieved with the multiphase space vector pulsewidth modulation (SVPWM) control technique [13] is less significant compared to sinusoidal pulsewidth modulation (SPWM). For example, by implementing the multiphase SVPWM control technique for nine-phase IM, the improvement in the linear modulation region by only 1.55% is achieved compared to SPWM control, whereas it is 15.4% in the case of the three-phase machine [13]. Further, some topologies with phase grouping technique are presented in [11], [14] to minimize the third-order harmonic content in phase currents. These topologies are controlled with three 3-phase SVPWMs, which improves the linear modulation region by 15.4%. However, these topologies require open-end winding PPM IM, additional isolated dc voltage sources, and high number of power semiconductor switches which may lead to higher cost.

To enhance the linear modulation region and reduce the harmonic content, a 12-sided polygon-based SVPWM control technique is presented in [15] for a six-phase IM. This technique helped in obtaining the improved linear modulation region. The similar 12-sided polygon structure produced from the inverter structure for a three-phase IM is presented in [16]. This control technique eliminates the $6n \pm 1$ (n = odd) harmonics in the phase voltages and hence leads to the reduction in losses and minimization of torque pulsations. Later in the literature [17]–[19], an octadecagonal SVPWM is implemented using multilevel inverter configurations to achieve an enriched harmonic profile. However, this method has limitations regarding power circuit complexity, as well as requires a higher number of switches when applied to multiphase IM drives.

For achieving better harmonic profile in the high-pole mode and with increased linear modulation in low-pole mode, a nine-phase PPM IM drive is proposed in this article. The proposed method uses a nine-phase PPM IM and a basic two-level

Manuscript received May 8, 2019; revised July 30, 2019; accepted September 21, 2019. Date of publication October 15, 2019; date of current version April 30, 2020. *(Corresponding author: Sivakumar Keerthipati.)*

V. Janaki Ramaiah and S. Keerthipati are with the Department of Electrical Engineering, Indian Institute of Technology Hyderabad, Sangareddy 502285, India (e-mail: ee17resch11013@iith.ac.in; ksiva@iith.ac.in).

Color versions of one or more of the figures in this article are available online at http://ieeexplore.ieee.org.

Digital Object Identifier 10.1109/TIE.2019.2946537

TABLE I
OPERATING DETAILS FOR PERFORMANCE IMPROVEMENT OF NINE-PHASE IM

PPM Mode	Control Technique	Frequency range (Hz)	Speed range (rpm)
3-phase 12-pole	Hexagonal SVPWM	0-50	0-500
9-phase 4-pole	Octadecagonal SVPWM	16.67-50	500-1500

nine-leg inverter structure which reduces the power circuit complexity. The article is organized as follows: the performance enhancement of nine-phase IM using the proposed methodology is presented in Section II. The operation of nine-phase IM using carrier-based hexagonal SVPWM and octadecagonal SVPWM control is also presented in Section II [20]. The finite-element model (FEM) and experimental results, in order to fortify the proposed methodology, are presented in Section III. Section IV concludes this article.

II. PERFORMANCE ENHANCEMENT OF NINE-PHASE PPM IM DRIVE USING THE PROPOSED HYBRID CONTROL OPERATION

As discussed above, in order to achieve better performance over the entire speed range, hexagonal SVPWM and octadecagonal SVPWM control techniques are implemented during the low-speed and high-speed regions, respectively. The operating details of the nine-phase IM according to the proposed concept are presented in Table I.

As given in Table I, for speeds below 500 r/min, the PPM IM drive is operated in 3-phase 12-pole mode, where the machine gives the flexibility for the implementation of hexagonal SVPWM control technique. In this mode, to achieve the variable speeds below 500 r/min, the fundamental frequency is varied from 0 to 50 Hz, and the reference voltage vector is varied with the modulation index from 0 to 1. For speeds between 500 and 1500 r/min, the PPM IM drive is operated in nine-phase four-pole mode by implementing the octadecagonal SVPWM control technique. In this mode, to achieve variable speeds, the fundamental supply frequency is varied from 16.67 to 50 Hz, and the reference voltage vector is varied with the modulation index from 0.33 to 1. This operation makes sure of the improvement in the harmonic profile during low-speed operating region. In addition, the implementation of octadecagonal SVPWM control during high-speed region improves the linear modulation region.

The reference vector is close to the adjacent vectors of a sector in octadecagon SVPWM (sector angle = 20°) compared to that in the hexagonal SVPWM (sector angle = 60°), resulting in the production of less error vector [10]. Thus, the harmonic profile obtained using octadecagonal SVPWM is better compared to hexagonal SVPWM. However, with the reduction in the modulation index, the harmonics generated using octadecagonal SVPWM will also increase which in turn generates more torque pulsations in the motor [21]. To overcome this issue, during the lower modulation index, the hexagonal SVPWM control is implemented by operating the nine-phase IM drive in 3-phase 12-pole mode. By this operation, the reference

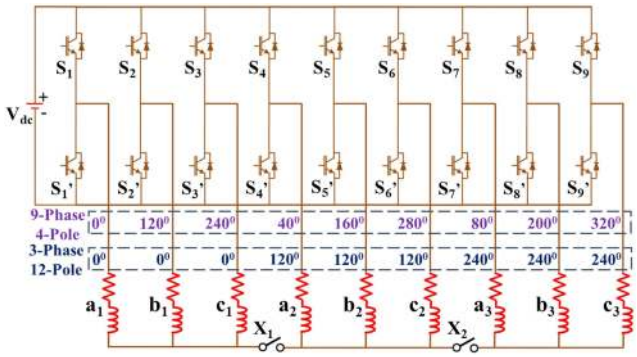

Fig. 1. Inverter structure of nine-phase PPM IM drive for both 9-phase 4-pole and 3-phase 12-pole modes of operations.

vector which has been in the lower modulation region (less than 0.33) of octadecagonal SVPWM (producing more harmonics) is shifted close to the unity modulation index in the hexagonal SVPWM producing a better harmonic profile. This operation further results in the reduced torque pulsations. To show the effectiveness of the proposed method, the harmonic content [in terms of total-harmonic distortion (THD)] produced by using hexagonal SVPWM control for 3-phase 4-pole operation, octadecagonal SVPWM control for 9-phase 4-pole operation, hexagonal SVPWM control for 3-phase 12-pole operation, and the proposed methodology is compared, as presented in Table II. A switching frequency of 2050 Hz (odd multiples of the fundamental frequency) is used for the calculation of THD. From Table II, it can be clearly observed that the harmonic content produced by using the proposed method, for different operating speeds, is less compared to that produced by using the other three control techniques.

The nine-phase PPM IM is excited with a basic two-level nine-leg inverter, and the excitation angles for both the 9-phase 4-pole and 3-phase 12-pole modes of operation are displayed in Fig. 1. The phase grouping and excitation details for achieving the 9-phase 4-pole and 3-phase 12-pole modes are presented in [11]. The detailed operation of the nine-phase PPM IM using octadecagonal SVPWM and hexagonal SVPWM control techniques is explained below.

A. Hexagonal SVPWM Operation During the Low-Speed Region

In the lower modulation region, the carrier-based hexagonal SVPWM control is implemented by operating the nine-phase PPM IM in 3-phase 12-pole mode. During the 3-phase 12-pole mode of operation, the four-quadrant switches (X_1 and X_2) are turned ON resulting in a common neutral. This operation results in the formation of three overlapped hexagonal voltage space vector structure with a vector length of "V_{dc}." The three overlapped hexagonal voltage space vector structure is shown in Fig. 2(a). The combination of three overlapped hexagons will result in a new hexagonal voltage space vector structure with a vector length of 3 V_{dc} and is as shown in Fig. 2(b). In Fig. 2(b), "Vs" represents the reference voltage space vector and "θ" is the

TABLE II
COMPARISON TABLE SHOWING THE EFFECTIVENESS OF PROPOSED METHODOLOGY

Speed	Hexagonal SVPWM for 3-phase 4-pole machine		Octadecagonal SVPWM for 9-phase 4-pole machine			Hexagonal SVPWM for 3-phase 12-pole machine		Proposed method			
	MI	THD (%)	MI	Phase voltage (Va1) THD (%)	Equivalent winding voltage (a1, a2, a3) THD (%)	MI	THD (%)	Mode	SVPWM control technique	MI	THD (%)
1500	1	52.31	1	33.76	20.07	NA	NA	4-pole	Octadecagon	1	20.07
1200	0.8	76.92	0.8	62.64	54.79	NA	NA	4-pole	Octadecagon	0.8	54.79
900	0.6	105.94	0.6	92.50	85.62	NA	NA	4-pole	Octadecagon	0.6	85.62
600	0.4	147.73	0.4	133.58	126.49	NA	NA	4-pole	Octadecagon	0.4	126.49
450	0.3	180.12	0.3	164.67	157.03	0.9	64.36	12-pole	Hexagon	0.9	64.36
300	0.2	231.67	0.2	213.77	204.97	0.6	105.94	12-pole	Hexagon	0.6	105.94
150	0.1	342.50	0.1	318.28	306.48	0.3	180.12	12-pole	Hexagon	0.3	180.12

MI, modulation index; NA, not applicable; THD, total harmonic distortion (by considering the harmonics up to Nyquist frequency).

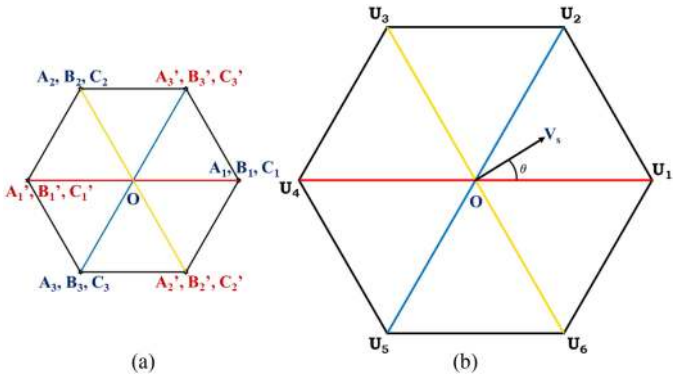

Fig. 2. (a) Three overlapped hexagonal voltage space vector structures. (b) Equivalent hexagonal voltage space vector structure.

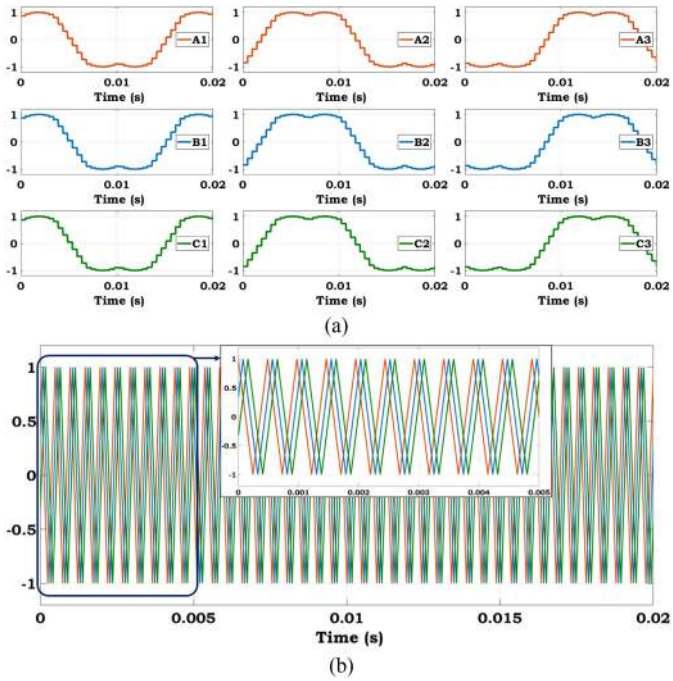

Fig. 3. (a) Modulating waveforms and (b) three triangular carrier waveforms phase-shifted by 60° used during the application of 3-phase 12-pole mode of operation.

angle made by "Vs" with respect to "V_1." The maximum length of the reference space vector realized in the linear modulation region of the hexagon is $3V_{dc} \times \cos(30°) = 2.5981\ V_{dc}$. The maximum phase voltage obtained using hexagonal SVPWM is $(2/9) \times (2.5981\ Vdc) = 0.5773\ V_{dc}$ [13], [22]. The reference voltage space vector, "Vs," can be realized by the two adjacent voltage vectors in a sector and zero vector, "O" at the center. For an instance, when "Vs" is in Sector-1, within a sampling time period of "Ts," it can be realized by switching between starting state, "U_1," of the sector and ending state, "U_2," of the sector and the zero vector, "O," for the time periods T_1 T_2, and T_0, respectively. Each of the possible zero vectors [$(+++)$ and $(---)$] of every group is switched for a period of (T_0/2). The equations to determine the time periods in the "nth" sector are as presented in (1). This results in the generation of the modulating waveforms as presented in Fig. 3(a).

$$T_1 = \left|\frac{\vec{V_s}}{3V_{dc}}\right| \frac{T_s \sin(n \times 60° - \theta)}{\sin(60^0)}$$
$$T_2 = \left|\frac{\vec{V_s}}{3V_{dc}}\right| \frac{T_s \sin(\theta - (n-1) \times 60°)}{\sin(60°)}.$$
$$T_0 = T_s - (T_1 + T_2) \quad (1)$$

The space harmonics will be high due to less number of phases which results in high torque ripple. The basic two-level phase voltage waveform has high harmonic content which further results in increased torque ripple. To improve the torque profile, multilevel phase voltage waveform has been generated by using carrier phase-shift technique [11], [12], [14], [23]. In 3-phase 12-mode of operations, the phase windings of nine-phase PPM IM machine act as equal voltage profile coils (EVPC) [23].

Each phase is contributed by a combination of three EVPCs. Phase windings (a_1, b_1, c_1) act as EVPCs for R-phase, phase windings (a_2, b_2, c_2) act as EVPCs for Y-phase, and phase windings (a_3, b_3, c_3) act as EVPCs for B-phase. The effective phase voltage is given by the algebraic sum of voltages across

their respective EVPCs. The hexagonal SVPWM modulating waveform with 50 Hz frequency and three triangular carrier waveforms phase-shifted by 60° with 2050 Hz frequency used for the generation of pulses are shown in Fig. 3. In carrier phase-shift method, three triangular carriers displaced by 60° are used for three EVPCs of each phase to generate a multilevel voltage across each phase. Phase windings a_1, a_2, and a_3 are switched using a 0° phase-displaced carrier which results in zero-sequence voltage with 0° phase displacement. Similarly, zero-sequence voltage with 60° phase displacement is produced by switching the phase windings b_1, b_2, and b_3 with 60° phase-displaced carriers and zero-sequence voltage with 120° phase displacement is produced by switching the phase windings c_1, c_2, and c_3 with 120° phase-displaced carriers. The interaction of the three phase-shifted zero-sequence voltages (due to common neutral) degrades the harmonic profile of EVPCs voltage. However, the respective sum of the voltage across EVPCs results in a multilevel voltage with seven levels for unity modulation index which is considered as the voltages across phases R, Y, and B [24]. As the multilevel voltage waveforms across phases have a better harmonic profile, the torque pulsations in the machine are reduced.

B. Octadecagonal SVPWM Operation During the High-Speed Region

In the higher speed region, the machine can be controlled with hexagonal SVPWM control as presented in [11], [14], where the linear modulation region is improved by 15.4% as compared to SPWM control. To further improve the linear modulation region, octadecagonal SVPWM is implemented by operating the nine-phase PPM IM drive in 9-phase 4-pole mode. The four-quadrant switches (X_1 and X_2) are turned OFF during nine-phase four-pole mode leading to the formation of three isolated neutrals. The isolated neutrals help avoiding the flow of circulating current through phase windings. Analytically, the nine-phase windings can be considered as three 3-phase winding groups. The phase windings (a_1, b_1, c_1) are considered as the first group, (a_2, b_2, c_2) as the second group, and (a_3, b_3, c_3) as the third group. In every group, the windings are displaced with a phase-shift of 120°. With the first group as a reference, the second and third groups are displaced with a phase-shift of 40° and 80°, respectively. Each of the three-phase groups results in a hexagonal voltage space vector structure with a vector length of V_{dc}. The hexagonal structures formed by the second group and the third group will be phase-shifted by 40° and 80°, respectively, with the hexagonal structure formed by the first group. The three hexagonal voltage space vector structures for the 9-phase 4-pole mode are as shown in Fig. 4(a). Adding the combination of three adjacent vectors (say $\overrightarrow{OB'_2}$, $\overrightarrow{OA_1}$, and $\overrightarrow{OB'_3}$) will result in a new vector ($\overrightarrow{OV_1}$) of length 2.8794 V_{dc}. The octadecagonal voltage space vector structure is obtained by joining all the resultant vectors ($\overrightarrow{OV_1}$ to $\overrightarrow{OV_{18}}$) formed by 18 different possible combinations of adjacent vectors as shown in Fig. 4(b). The maximum length of the reference space vector realized in the linear modulation region of octadecagon is 2.8794 $V_{dc} \times \cos(10°) = 2.8357\ V_{dc}$. With the octadecagonal SVPWM control, the maximum phase voltage obtained is (2/9) × (2.8357 V_{dc}) = 0.6302 V_{dc}. The maximum phase voltage obtained with the conventional SPWM is 0.5 V_{dc} and with the conventional three-phase SVPWM is 0.5773 V_{dc}. Hence, with the octadecagonal SVPWM control, the linear modulation region is improved by 26.03% compared to conventional SPWM control and 9.15% compared to conventional three-phase SVPWM control.

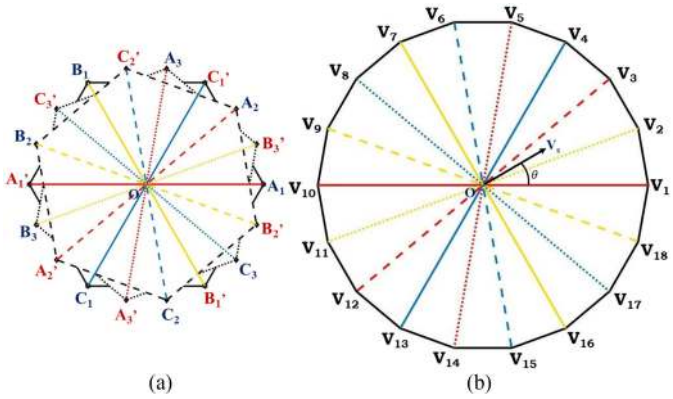

Fig. 4. (a) Individual hexagonal voltage space vector structures of three phase groups phase-shifted by 40°. (b) Octadecagonal voltage space vector structure for 9-phase 4-pole mode of operation.

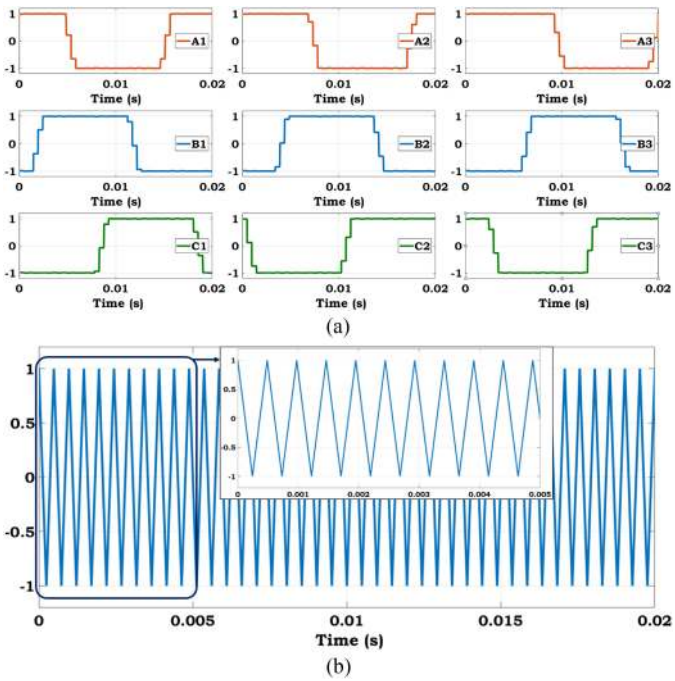

Fig. 5. (a) Modulating waveforms and (b) triangular carrier waveform used during the application of 9-phase 4-pole mode of operation.

In Fig. 4(b), "Vs" represents the reference voltage space vector and "θ" is the angle made by "Vs" with respect to starting vector state in the sector. The reference voltage space vector, "Vs," can be realized by the two adjacent voltage vectors in a sector and zero vector, "O," at the center. For instance, when "Vs" is in Sector-1, within a sampling time period of "Ts," it

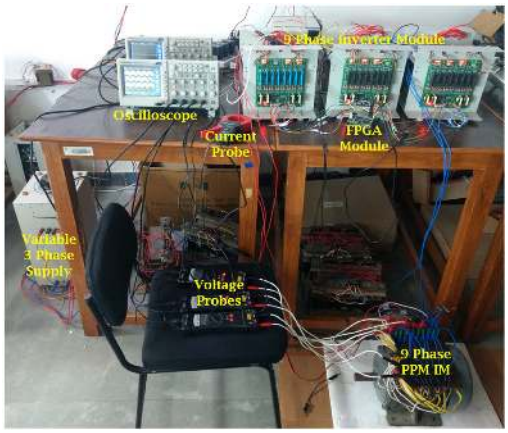

Fig. 6. Experimental setup used in the laboratory.

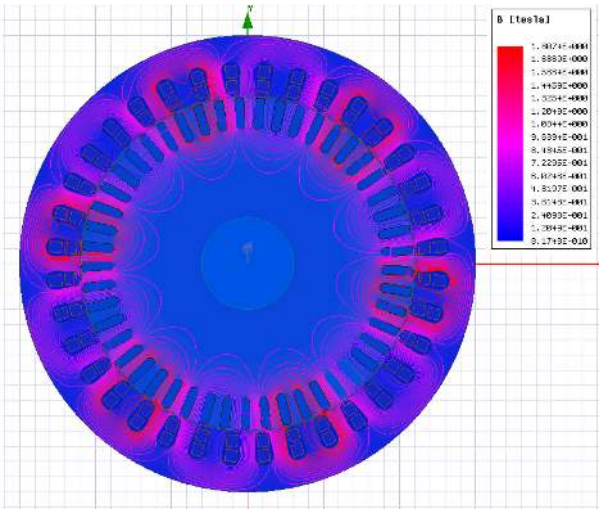

Fig. 7. Magnetic field density and its flux lines obtained during the application of 3-phase 12-pole mode of operation.

can be realized by switching between starting state, "V_1," of the sector and ending state, "V_2," of the sector, and the zero vector, "O," for the time periods T_1, T_2, and T_0, respectively. Each of the possible zero vectors [(+ + +) and (− − −)] of every group is switched for a period of (T_0/2). The equations to determine the time periods in "nth" sector are as presented in (2). This results in the generation of the modulating waveforms as presented in Fig. 5(a). The modulating octadecagonal SVPWM waveform with 50 Hz frequency and triangular carrier waveform with 2050 Hz frequency used for generation of pulses are presented in Fig. 5.

$$T_1 = \left|\frac{\vec{V_s}}{2.8794V_{\rm dc}}\right| \frac{T_s \sin\left(n \times 20^\circ - \theta\right)}{\sin\left(20^\circ\right)}$$

$$T_2 = \left|\frac{\vec{V_s}}{2.8794V_{\rm dc}}\right| \frac{T_s \sin\left(\theta - (n-1) \times 20^\circ\right)}{\sin\left(20^\circ\right)}.$$

$$T_s = T_0 + T_1 + T_2 \tag{2}$$

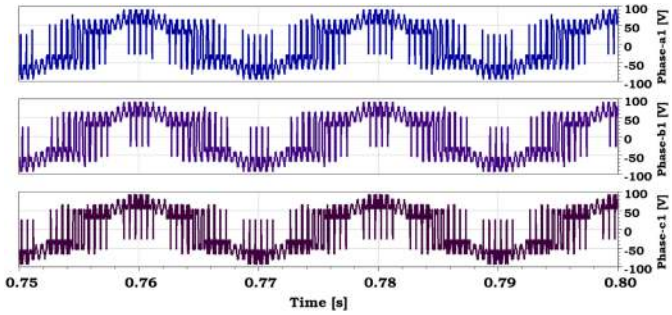

Fig. 8. Simulation results of voltage across individual phase windings a_1, b_1, c_1 obtained during the application of 3-phase 12-pole mode of operation.

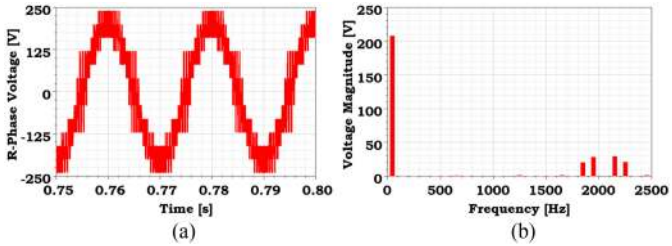

Fig. 9. Simulation results obtained during the application of 3-phase 12-pole mode of operation. (a) Algebraic sum of voltages across phase windings a_1, b_1, c_1 and (b) its harmonic profile.

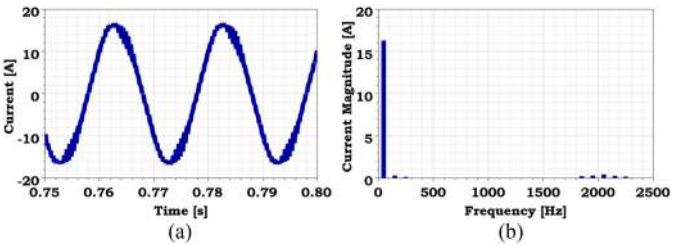

Fig. 10. Simulation results obtained during the application of 3-phase 12-pole mode of operation. (a) Current through phase-a_1 winding and (b) its harmonic profile.

With the octadecagonal SVPWM, the $18n \pm 1$ (where $n = 1, 2, 3, \ldots$) harmonics are absent in the phase voltages [10]. The dominant lower order harmonics in the phase voltage are 3rd, 5th, 7th, 11th, and 13th . . . . However, the triplen harmonic components in the phase voltages and currents can be eliminated by using phase grouping technique and with the isolated neutrals [11], [14]. Besides, the 5th, 7th, 11th, and 13th harmonic components do not contribute to the total flux in the air gap due to the winding disposition [10], [15], [25], [26]. Thus, a significant reduction in the torque ripple is achieved.

III. FEM Simulation and Experimental Results

The FEM model of nine-phase PPM IM is simulated using ANSYS Maxwell 2-D. To achieve 5-hp power rating, the machine parameters like core length, air-gap diameter, and air-gap length are effectively designed as 220, 170, and 0.35 mm,

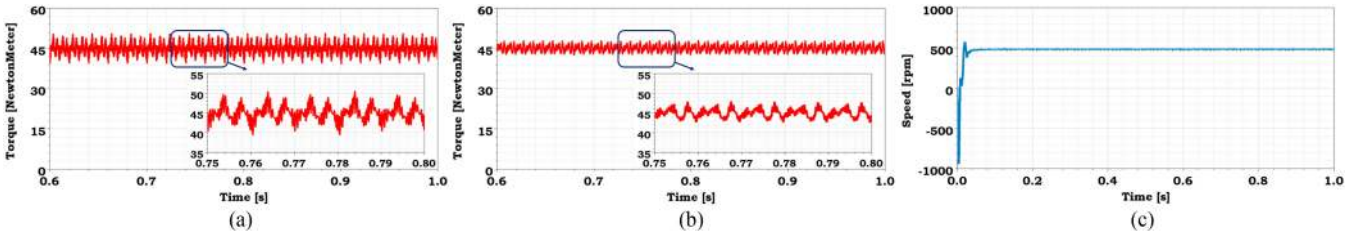

Fig. 11. Simulation results obtained during the application of 3-phase 12-pole mode of operation. (a) Rotor torque profile using carrier-based hexagonal SVPWM control technique with single triangular carrier waveform. (b) Rotor torque profile using carrier-based hexagonal SVPWM control technique with three triangular carrier waveforms phase-shifted by 60°. (c) Rotor speed.

respectively. The 2-level 9-leg inverter structure is designed in Simplorer environment. The integration of the 2-level 9-leg inverter model and nine-phase PPM IM machine model is done by using co-simulation. The triangular meshing is used for the FEM model simulation.

The simulation results obtained using FEM analysis are validated experimentally on a 5-hp machine in the laboratory. The experimentation is performed on the 5-hp nine-phase PPM IM in the open-loop mode due to laboratory constraints. The experimental setup is as shown in Fig. 6. The dc source is modeled by using three-phase rectifier module (SBR3510) at the output of a three-phase ac variable supply. The dc-link capacitor (2200MFD 450VDC) is used to reduce the voltage ripple at the output of the rectifier. A dc-link voltage of 120 V and carrier frequency of 2050 Hz (odd multiples of the fundamental frequency) are considered for both the simulation and experimentation purpose due to laboratory constraints. The nine legs of inverter structure are formed by using nine semikron SKM50GB128D insulated-gate bipolar transistor (IGBT) modules with their corresponding gate driver modules. The gate pulses with a deadband of 2 μs have been generated by using very high speed integrated circuit hardware description language (VHDL) coding on XILINX SPARTAN-6 (XC6SLX9) field-programmable gate array (FPGA) hardware platform.

A. Lower Speed Region

In the lower modulation region, the machine is operated in 3-phase 12-pole mode and hexagonal SVPWM control technique is used. The magnetic field distribution forming 12 poles over the entire cross section of the machine is as shown in Fig. 7. The simulation results of voltage across the individual phase windings a_1, b_1, and c_1 are as shown in Fig. 8. The simulation results of R-phase voltage (algebraic sum of the voltage across phase windings a_1, b_1, and c_1) and its corresponding harmonic spectrum are as presented in Fig. 9(a) and (b), respectively. The current through the phase winding a_1 and its harmonic profile is as presented in Fig. 10(a) and (b), respectively. From the harmonic profiles of total effective voltage, it can be observed that the dominating harmonics are present at the switching frequency. The rotor torque profile using the carrier-based hexagonal SVPWM control technique with single triangular carrier waveform [20] and with three triangular carrier waveforms phase-shifted by 60° is as presented in Fig. 11(a) and (b), respectively. The torque ripple in Fig. 11(a) and (b) is calculated to be 24% and 12.20%, respectively. This shows that the performance is improved with the hexagonal SVPWM control technique using carrier phase-shift method. The speed profile of nine-phase PPM IM during the application of 3-phase 12-pole mode of operation is as presented in Fig. 11(c) which shows the steady-state operation of the machine.

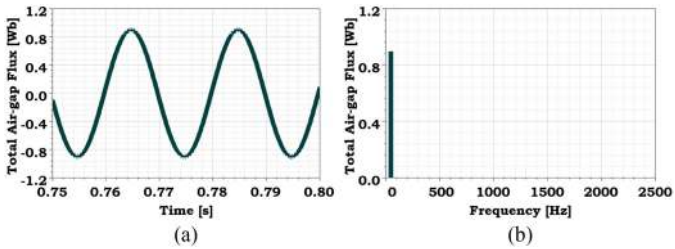

Fig. 12. Simulation results obtained during the application of 3-phase 12-pole mode of operation. (a) Total air-gap flux. (b) Harmonic profile of total air-gap flux.

The total air-gap flux in the nine-phase IM along with its harmonic profile during the 3-phase 12-pole mode of operation is given in Fig. 12. From the harmonic profile of the total air-gap flux, it can be observed that the harmonics in the individual phase voltages and currents are not reflected in total air-gap flux. The experimental results of voltages across individual phase windings (a_1, b_1, and c_1), the algebraic sum of the voltages across phase windings a_1, b_1, c_1, and current through phase winding-a_1 are presented in Fig. 13. From Fig. 13, multilevel voltage is observed (the red color trace) in Fig. 13(a) which represents the algebraic sum of three-phase windings a_1, b_1, c_1. The harmonic profiles of resultant voltage and current through phase winding-a1 are presented in Fig. 13(b) and (c), respectively.

B. Higher Speed Region

In the higher speed region, the machine is operated in the nine-phase four-pole mode and octadecagonal SVPWM control technique is used. The magnetic field distribution over the entire cross section of the machine during this mode of operation is as shown in Fig. 14.

The formation of four poles over the cross section of the machine can be observed in Fig. 14. The FEM simulation

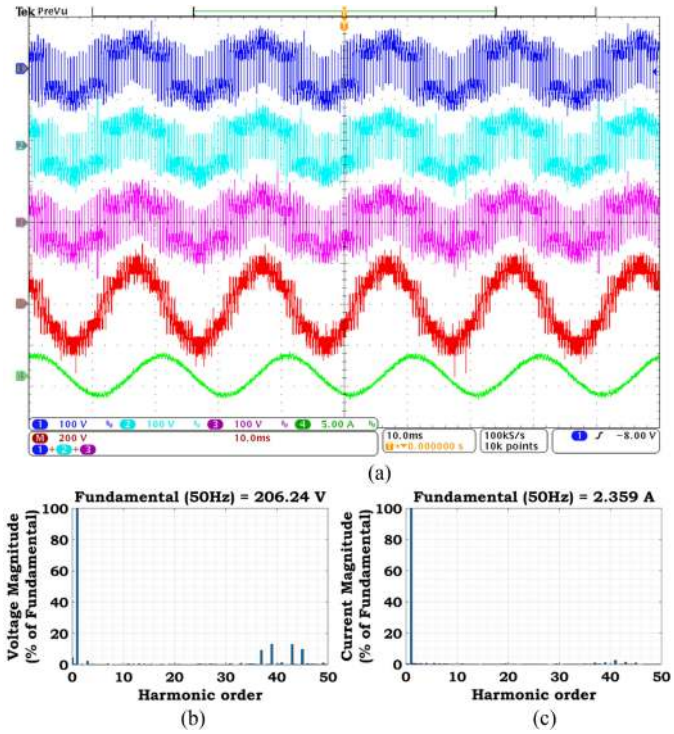

Fig. 13. Experimental results obtained during the application of 3-phase 12-pole mode of operation. (a) Voltage across individual phase windings a_1, b_1, c_1 (*top 3 traces respectively, X-axis:* 10 ms/div *and Y-axis:* 100 V/div), algebraic sum of voltages across phase windings a_1, b_1, c_1 (fourth trace, *X-axis:* 10 ms/div *and Y-axis:* 200 V/div), and current through phase-a_1 winding (*bottom trace, X-axis:* 10 ms/div *and Y-axis:* 5 A/div). (b) Harmonic profile of resultant voltage of phase windings a_1, b_1, c_1. (c) Harmonic profile of current through phase-a_1 winding.

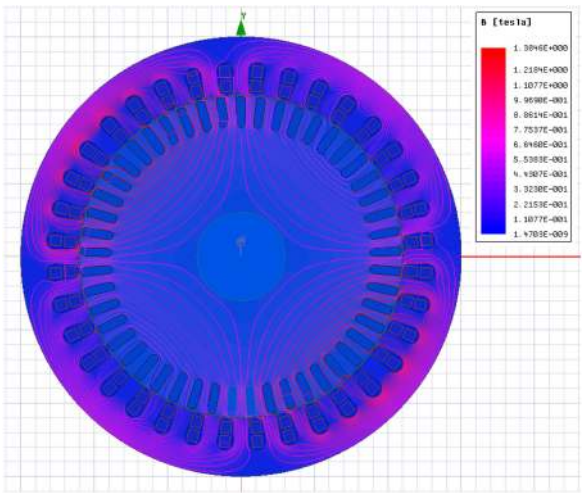

Fig. 14. Magnetic field density and its flux lines obtained during the application of 9-phase 4-pole mode of operation.

results of phase voltage and current waveform including their harmonic profiles are shown in Figs. 15 and 16, respectively. Even though the phase voltage and current waveforms contain 5th, 7th, 11th, and 13th harmonics, these do not reflect in the effective air-gap flux due to the winding disposition

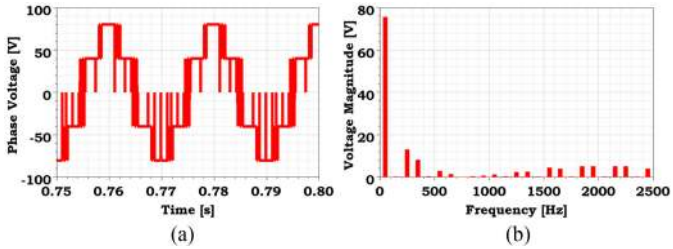

Fig. 15. Simulation results obtained during the application of 9-phase 4-pole operation. (a) Voltage across phase-a_1 winding. (b) Voltage harmonic profile.

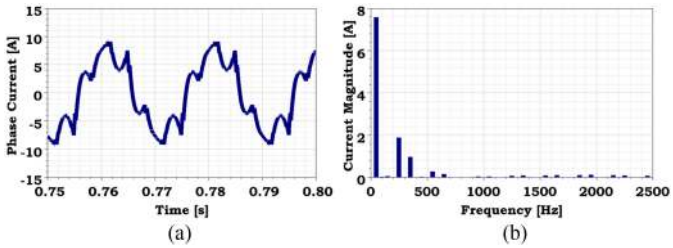

Fig. 16. Simulation results obtained during the application of nine-phase four-pole operation. (a) Current through phase-a_1 winding. (b) Current harmonic profile.

[15], [25], [26] resulting in the reduction of torque ripple. As the air-gap flux does not contain harmonics of the order 5th, 7th, 11th, and 13th . . . , there is no back electromotive force (EMF) generated in the phase windings due to these respective harmonic orders. The absence of back EMF in the phase windings results in the presence of the harmonics of the order 5th, 7th, 11th, and 13th . . . in the phase currents. The torque profile using three individual hexagonal SVPWM and octadecagonal SVPWM control techniques is presented in Fig. 17(a) and (b), respectively. The torque ripple percentage in Fig. 17(a) and (b) during the steady state is calculated to be of 10% and 9.33%, respectively. The speed profile of nine-phase PPM IM during the application of nine-phase four-pole mode of operation is as presented in Fig. 17(c) which shows the steady-state operation of the machine. From Figs. 15 and 16, the lower order dominating harmonics in the harmonic profiles of individual phase voltage and phase currents can be observed. However, these harmonics do not reflect in the total air-gap flux of the nine-phase IM. This can be observed in Fig. 18, which shows the air-gap flux of nine-phase IM including its harmonic profile. The absence of lower order dominating harmonics in the total air-gap flux results in reduced torque pulsations. The experimental results of voltage across phase winding a_1 and current through it are shown in Fig. 19. From the harmonic profile of phase voltage and current presented in Fig. 19(b) and (c), it is observed that the 17th- and 19th-order harmonic components are of less magnitude. For a dc-link voltage of 120 V, the fundamental peak value of phase voltage obtained is 75.52 V, implying a dc-link voltage utilization of 0.62933 ($\approx$0.63) with the octadecagonal SVPWM control technique.

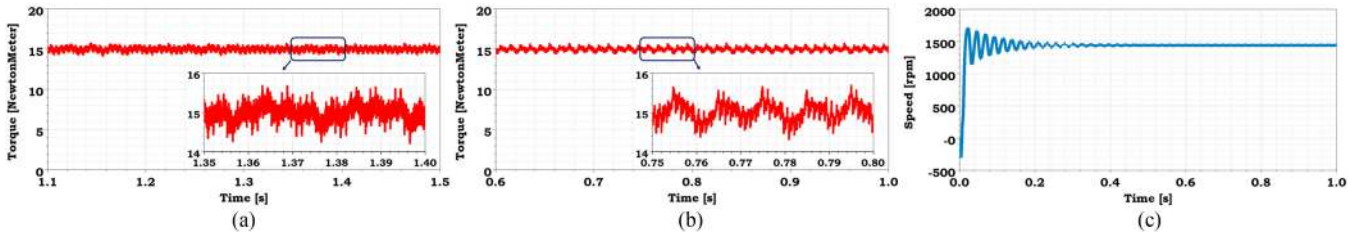

Fig. 17. Simulation results obtained during the application of 9-phase 4-pole operation. (a) Rotor torque profile using three individual hexagonal SVPWM control technique [11]. (b) Rotor torque profile using the proposed octadecagonal SVPWM control technique. (c) Rotor speed.

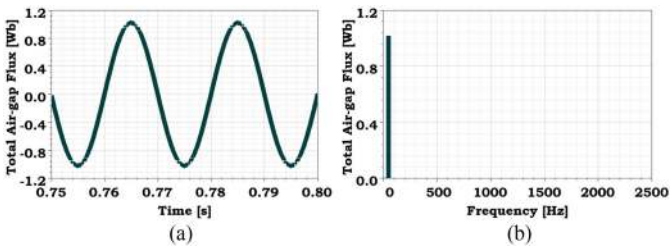

Fig. 18. Simulation results obtained during the application of 9-phase 4-pole operation. (a) Total air-gap flux. (b) Harmonic profile of total air-gap flux.

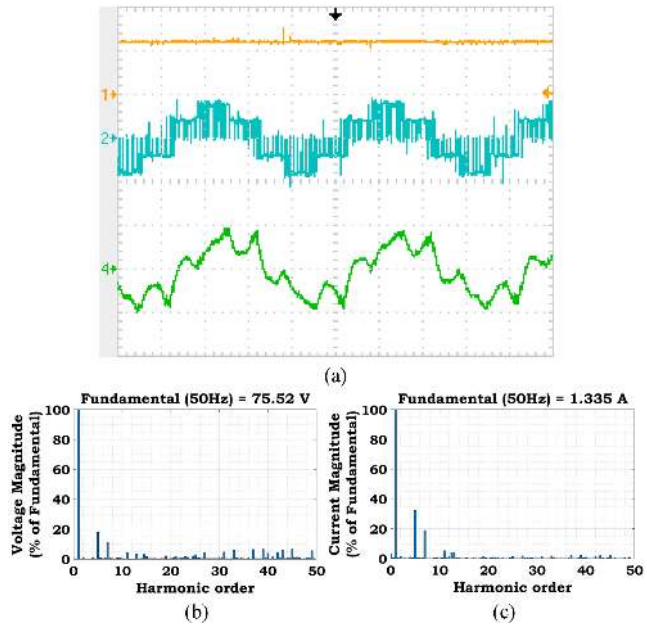

Fig. 19. Experimental results obtained during the application of 9-phase 4-pole mode of operation. (a) DC-link voltage (*top trace, X-axis:* 5 ms/div *and Y-axis:* 100 V/div), *voltage (middle trace, X-axis:* 5 ms/div *and Y-axis:* 100 V/div) *across phase-a*$_1$ *winding, and current (bottom trace, X-axis:* 5 ms/div *and Y-axis:* 2 A/div) *through phase-a*$_1$ winding. (b) Harmonic profile of voltage across phase-a$_1$ winding. (c) Harmonic profile of current through phase-a$_1$ winding.

IV. Conclusion

The hybrid control operation of nine-phase PPM IM drive using carrier-based hexagonal SVPWM and octadecagonal SVPWM control techniques was proposed in this article. To achieve the higher torque, the PPM IM was operated in the 3-phase 12-pole mode, and to get higher speed, the same machine was operated in the 9-phase 4-pole mode. The hexagonal SVPWM and octadecagonal SVPWM control techniques were effectively used for controlling the PPM IM drive in 3-phase 12-pole and 9-phase 4-pole modes of operation, respectively. In addition, octadecagonal SVPWM improved the linear modulation region by 26% compared to the conventional SPWM and 9.15% compared to the three individual hexagonal SVPWM control techniques. This hybrid control operation is best suitable for electric vehicle applications.

References

[1] C. Wenping, B. C. Mecrow, G. J. Atkinson, J. W. Bennett, and D. J. Atkinson, "Overview of electric motor technologies used for more electric aircraft (MEA)," *IEEE Trans. Ind. Electron.*, vol. 59, no. 9, pp. 3523–3531, Sep. 2012.

[2] M. Mengoni, L. Zarri, A. Tani, L. Parsa, G. Serra, and D. Casadei, "High torque-density control of multiphase induction motor drives operating over a wide speed range," *IEEE Trans. Ind. Electron.*, vol. 62, no. 2, pp. 814–825, Feb. 2015.

[3] I. Gonzalez-Prieto, M. J. Duran, H. S. Che, E. Levi, M. Bermúdez, and F. Barrero, "Fault-tolerant operation of six-phase energy conversion systems with parallel machine-side converters," *IEEE Trans. Power Electron.*, vol. 31, no. 4, pp. 3068–3079, Apr. 2016.

[4] E. Levi, R. Bojoi, F. Profumo, H. A. Toliyat, and S. Williamson, "Multiphase induction motor drives—A technology status review," *IET Elect. Power Appl.*, vol. 1, no. 4, pp. 489–516, Jul. 2007.

[5] J. W. Kelly and E. G. Strangas, "Torque control during pole-changing transition of a 3:1 pole induction machine," in *Proc. Int. Conf. Electr. Mach. Syst.*, Oct. 2007, pp. 1723–1728.

[6] B. Ge, D. Sun, W. Wu, and F. Z. Peng, "Winding design, modeling, and control for pole-phase modulation induction motors," *IEEE Trans. Magn.*, vol. 49, no. 2, pp. 898–911, Feb. 2013.

[7] S. Williamson and S. Smith, "Pulsating torque and losses in multiphase induction machines," *IEEE Trans. Industry Appl.*, vol. 39, no. 4, pp. 986–993, Jul./Aug. 2003.

[8] E. Levi, "Multiphase electric machines for variable-speed applications," *IEEE Trans. Ind. Electron.*, vol. 55, no. 5, pp. 1893–1909, May 2008.

[9] B. P. Reddy, M. A. Rao, M. Sahoo, and S. Keerthipati, "A fault-tolerant multilevel inverter for improving the performance of a pole-phase modulated nine-phase induction motor drive," *IEEE Trans. Ind. Electron.*, vol. 65, no. 2, pp. 1107–1116, Feb. 2018.

[10] E. A. Klingshirn, "High phase order induction motors - Part I-Description and theoretical considerations," *IEEE Trans. Power Appl. Syst.*, vol. PAS-102, no. 1, pp. 47–53, Jan. 1983.

[11] B. S. Umesh and K. Sivakumar, "Dual-inverter-fed pole-phase modulated nine-phase induction motor drive with improved performance," *IEEE Trans. Ind. Electron.*, vol. 63, no. 9, pp. 5376–5383, Sep. 2016.

[12] B. P. Reddy and S. Keerthipati, "Linear modulation range and torque ripple profile improvement of PPMIM drives," *IEEE Trans. Power Electron.*, vol. 34, no. 12, pp. 12120–12127, Dec. 2019.

[13] J. W. Kelly, E. G. Strangas, and J. M. Miller, "Multiphase space vector pulse width modulation," *IEEE Trans. Energy Convers.*, vol. 18, no. 2, pp. 259–264, Jun. 2003.

[14] B. S. Umesh and K. Sivakumar, "Pole-phase modulated multiphase induction motor drive with reduced torque ripple and improved dc link utilization," *IEEE Trans. Power Electron.*, vol. 32, no. 10, pp. 7862–7869, Oct. 2017.
[15] K. Gopakumar, V. T. Ranganthan, and S. R. Bhat, "Split-phase induction motor operation from PWM voltage source inverter," *IEEE Trans. Industry Appl.*, vol. 29, no. 5, pp. 927–932, Sep./Oct. 1993.
[16] A. Das, K. Sivakumar, R. Ramchand, C. Patel, and K. Gopakumar, "A combination of hexagonal and 12-sided polygonal voltage space vector PWM control for IM drives using cascaded two-level inverters," *IEEE Trans. Ind. Electron.*, vol. 56, no. 5, pp. 1657–1664, May 2009.
[17] K. Mathew, K. Gopakumar, J. Mathew, N. A. Azeez, A. Dey, and L. Umanand, "Medium voltage drive for induction motors using multilevel octadecagonal voltage space vectors," *IEEE Trans. Power Electron.*, vol. 28, no. 7, pp. 3573–3580, Jul. 2013.
[18] S. Lakshminarayanan, G. Mondal, and K. Gopakumar, "Multilevel inverter with 18-sided polygonal voltage space vector for an open-end winding induction motor drive," in *Proc. EUROCON – Int. Conf. "Comput. Tool*," Warsaw, 2007, pp. 1810–1817.
[19] M. Boby, S. Arun Rahul, K. Gopakumar, L. Umanand, F. Blaabjerg, and S. Bhattacharya, "A low-order harmonic elimination scheme for induction motor drives using a multilevel octadecagonal space vector structure with a single DC source," *IEEE Trans. Power Electron.*, vol. 33, no. 3, pp. 2430–2437, Mar. 2018.
[20] K. Zhou and D. Wang, "Relationship between space-vector modulation and three-phase carrier-based PWM: A comprehensive analysis [three-phase inverters]," *IEEE Trans. Ind. Electron.*, vol. 49, no. 1, pp. 186–196, Feb. 2002.
[21] O. Dordevic, M. Jones, and E. Levi, "Analytical formulas for phase voltage RMS squared and THD in PWM multiphase systems," *IEEE Trans. Power Electron.*, vol. 30, no. 3, pp. 1645–1656, Mar. 2015.
[22] J. Holtz, "Pulsewidth modulation-A survey," *IEEE Trans. Ind. Electron.*, vol. 39, no. 5, pp. 410–420, Oct. 1992.
[23] B. S. Umesh and K. Sivakumar, "Multilevel inverter scheme for performance improvement of pole-phase-modulated multiphase induction motor drive," *IEEE Trans. Ind. Electron.*, vol. 63, no. 4, pp. 2036–2043, Apr. 2016.
[24] D. G. Holmes and B. P. McGrath, "Opportunities for harmonic cancellation with carrier-based PWM for a two-level and multilevel cascaded inverters," *IEEE Trans. Industry Appl.*, vol. 37, no. 2, pp. 574–582, Mar./Apr. 2001.
[25] Y. Zhao and T. A. Lipo, "Space vector PWM control of dual three-phase induction machine using vector space decomposition," *IEEE Trans. Industry Appl.*, vol. 31, no. 5, pp. 1100–1109, Sep./Oct. 1995.
[26] D. C. White and H. H. Woodson, *Electromechanical Energy Conversion*. New York, NY, USA: Wiley, pp. 545–593.

V. Janaki Ramaiah (S'19) received the B.Tech. degree in electrical and electronics engineering (EEE) from the Jawaharlal Nehru Technological University Anantapur College of Engineering Pulivendula, Kadapa, India, in 2013, and the M.Tech. degree in power electronics and power system, in 2016 from the Indian Institute of Technology Hyderabad, Sangareddy, India, where he is currently working toward the Ph.D. degree.

His research interests include multilevel inverters, multiphase induction machine drives, pole-phase modulation, and pulsewidth modulation techniques.

Sivakumar Keerthipati (M'12–SM'16) received the B.Tech. degree in electrical engineering from Sri Venkateswara University, Tirupati, India, in 2004, the M.Tech. degree in power electronics and drives from the National Institute of Technology, Warangal, India, in 2006, and the Ph.D. degree in power electronics and drives from the Center for Electronics Design and Technology, Indian Institute of Science, Bangalore, India, in 2010.

He is currently an Associate Professor with the Department of Electrical Engineering, Indian Institute of Technology Hyderabad, Sangareddy, India. His research interests include multilevel inverters, open-end winding induction motor drives, pulsewidth modulation techniques, switched-mode power conversion, microgrids, and power quality and control.

Dr. Keerthipati is the recipient of IETE Bimal K Bose award for the year 2018.